Coupled Processes Modeling in Rock Salt and Crushed Salt Including Halite Solubility Constraints: Application to Disposal of Heat-Generating Nuclear Waste

Laura Blanco-Martín[1,3], Jonny Rutqvist[1], Alfredo Battistelli[2], Jens T. Birkholzer[1]

[1] Energy Geosciences Division, Lawrence Berkeley National Laboratory, 1 Cyclotron Rd, MS 74R316C, Berkeley, CA 94720, USA [2] Risamb Department, Saipem SpA, Via Toniolo 1, 61032 Fano, PU, Italy [3] Present Address: MINES ParisTech, Department of Geosciences, PSL Research University, 35 rue Saint Honoré, 77300 Fontainebleau, France

Abstract

This paper presents numerical modeling of coupled thermal, hydraulic and mechanical processes in rock salt and crushed salt considering halite solubility constraints. The TOUGH-FLAC simulator is used, with a recently enhanced Equation-Of-State module that includes the thermodynamic properties of aqueous fluids of variable salinity. Laboratory and field scale tests performed on rock salt and crushed salt under temperature gradients are modeled first to evaluate the capabilities of the simulator to reproduce important features, such as porosity changes induced by halite dissolution/precipitation, and brine and heat migration. Since the results are quite satisfactory, the simulator is used to predict the long-term response of a generic salt repository for heat-generating nuclear waste. To evaluate the impacts of halite solubility on the predictions, two simulations that respectively consider or neglect solubility constraints are performed. In the scenario studied, the results are not significantly affected by dissolution/precipitation, and only some differences are observed due to changes in porosity, but the dominating processes remain the same. With the new provisions, TOUGH-FLAC is more complete in terms of processes occurring around a heat-releasing nuclear waste package and can therefore provide more accurate predictions of the long-term performance of a nuclear waste repository in salt formations.

Keywords: Natural and crushed salt · Halite solubility · THM processes · Nuclear waste disposal · Numerical modeling

1 Introduction

The underground disposal of nuclear waste requires the analysis of complex interactions between physical and chemical processes (Hou 2003; Hunsche and Hampel 1999; Stephansson et al. 2004; Tsang 1991; Wang et al. 2008; Wolters et al. 2012). In order to comply with safety requirements, the performance of a nuclear waste repository has to be evaluated over the long-

term (typically, thousands or even millions of years for heat-generating nuclear waste). Due to the complexity of the processes that need to be investigated, their interactions and the time scales considered, numerical modeling using proper tools and state-of-the art knowledge is required (Tsang et al. 2009).

In this study, we focus on the disposal of heat-generating nuclear waste in rock salt. Rock salt (mainly composed of halite, NaCl) is a potential disposal medium for the underground disposal of nuclear waste because of several favorable attributes, including near-zero permeability in the undisturbed state, very low porosity, and relative high thermal conductivity as compared to other shallow-crustal rock types. Additionally, rock salt creeps under deviatoric stresses and temperature changes, and has the capability to heal technically induced fractures if the stress state is propitious (Bechthold et al. 1999; Carter et al. 2011; Hardin and Voegele 2013). Moreover, saline formations are easy to mine and can be found underground in large volumes in geologically stable areas. The excavated, run-of-mine salt (crushed salt) can be used as backfill material. As the emplacement drifts close due to the creep of the host rock, the crushed salt backfill undergoes a reconsolidation process (Bechthold et al. 2004; Callahan et al. 1998; Hurtado et al. 1997; Wieczorek et al. 2012). During this process, porosity decreases from 30–40% to low residual values (< 10% in the long-term), and the mechanical and flow properties of the crushed salt evolve toward the characteristic values of the natural salt host rock. Once consolidated, it is expected that the crushed salt will provide an engineered barrier function, thereby reinforcing the geological barrier provided by the natural salt host rock (Bechthold et al. 2004).

In order to understand the behavior of the natural salt host rock and the backfill material under disposal conditions, experimental studies and modeling exercises have been carried out (Bechthold et al. 1999, 2004; Blanco-Martín et al. 2015a, 2016; Broome et al. 2014; Hou 2003; Korthaus 1998; Kröhn et al. 2015; Popp et al. 2001; Pudewills and Droste 2003; Schulze et al. 2001; Wolters et al. 2012). For modeling purposes, it is commonly assumed that Darcy flow holds for rock salt because attention is focused on non-undisturbed states (in the undisturbed state, Darcy's law can be applied as a first approximation, see Bérest et al. 1999). Within the host rock, these investigations address damage (dilatancy, fluid permeation and the development of secondary permeability and porosity) as well as healing (damage reduction and recovery of the barrier integrity), and within the crushed salt, they study the reconsolidation process (evolution of flow and mechanical properties during compaction). In some of these investigations, halite solubility constraints are accounted for; indeed, halite is very soluble in

water, and solubility increases with temperature. Along with salt dissolution, the porosity increases, leading to changes in key parameters such as permeability (Rege and Fogler 1989). Conversely, as temperature decreases the solubility decreases, leading to the formation of a salt precipitate and a reduction in porosity and permeability. Some tests have been carried out to quantify brine migration and salt dissolution/precipitation effects. In the early 1980s, Nowak and McTigue (1987) performed several brine release tests in boreholes drilled in rooms A1 and B at WIPP, and observed that the amount of released brine increased with the applied heat load. Strain measurements in the boreholes also revealed faster convergence rates with increasing borehole wall temperature. At the laboratory scale, Olivella et al. (2011) applied a temperature gradient to cylindrical crushed salt samples and observed a clear non-uniform porosity evolution along the samples. Stauffer et al. (2013) conducted several bench-scale experiments on intact salt crystals and crushed salt, including a thermal test on a pile of run-of-mine salt with temperature measurements at different depths. From the modeling perspective, Jordan et al. (2015) simulated a salt repository including halite dissolution/precipitation effects and also a dehydration model of hydrous minerals (often present in impure salt). The authors focused on the crushed salt in the short-term, and showed that with sufficient amount of water a heat pipe can develop around the canisters, leading to different porosity, thermal conductivity, temperature and saturation evolution as compared to a case with little water present. However, from the long-term performance perspective, the modeled time was very short (460 days), and the simulations did not include mechanical effects or important coupled processes within the host rock and the crushed salt (thermo-mechanical damage, fluid permeation, healing, backfill reconsolidation).

In this paper, we present numerical modeling of coupled thermal, hydraulic and mechanical (THM) processes in rock salt and crushed salt accounting for halite solubility constraints. This work augments recent simulations from the authors in which halite dissolution/precipitation effects were neglected (Blanco-Martín et al. 2015a, b, 2016). The coupled THM simulations are performed with TOUGH-FLAC (Rutqvist et al. 2002; Rutqvist 2017), which is based on linking the multiphase flow and heat transport simulator TOUGH2 (Pruess et al. 2011) with the geomechanical simulator FLAC3D (Itasca 2012). A recently improved version of the EWASG Equation-Of-State (EOS) module of TOUGH2 is used in the flow sub-problem (Battistelli 2012). We first present this EOS and the enhancements required in TOUGH-FLAC to account for halite dissolution/precipitation. Subsequently, experimental data of natural salt and crushed salt under temperature gradients (laboratory and field scales) are compared against numerical predictions obtained using the enhanced version of TOUGH-FLAC. The tests mentioned above, performed by

Nowak and McTigue (1987), Olivella et al. (2011) and Stauffer et al. (2013), are used as test cases with comparison of numerical and experimental results. Since the agreement is quite satisfactory, this simulator is used to predict the long-term response (100,000 years) of a generic salt repository for heat-generating nuclear waste. To identify the impacts of halite solubility constraints on the predictions, two simulations that respectively include or neglect such constraints are carried out. Given that the focus is on a generic (i.e., not site-specific) repository, it is assumed that the amount of hydrous minerals within the salt is small. Although the results cannot be validated based on measurement data of the physical processes in the scenario considered, they suggest that halite dissolution/precipitation does not affect the long-term response significantly. The backfill evolution is dominated by mechanical compaction, and within the host rock the same processes occur (dilatancy, fluid permeation, healing), and only some differences in the permeability evolution are observed due to changes in porosity induced by dissolution/precipitation. With the new provisions implemented in TOUGH-FLAC, this simulator can be used to investigate more accurately the long-term disposal of heat-generating nuclear waste in salt-based formations.

2 Materials and Methods

2.1 Modeling of Halite Dissolution/Precipitation

Dissolution of halite in water results in brine. When halite and brine are taken into account in the simulations, some arrangements are necessary as compared to simpler water–air flow. First, the flow mixture has a third component, NaCl, and owing to precipitation, a third, solid phase has to be considered; the amount of this phase (i.e., the solid saturation) increases with NaCl precipitation and decreases with NaCl dissolution. While the gas and liquid phases are composed of air, water and NaCl, the solid phase is composed solely by NaCl. Due to the addition of a third component, an additional mass balance equation has to be solved.

Second, from the flow perspective the solid phase is immobile, i.e., there is no mass transport of solid halite. This particularity introduces the concept of an effective porosity (or active flow porosity), defined as the pore space occupied by the liquid and the gas phases (i.e., the mobile phases). On the other hand, the total porosity (ratio of pore volume to total volume) includes the solid phase. The relationship between the effective and the total porosities is

$$\phi_{\text{eff}} = \phi\,(1 - S_s) \tag{1}$$

where ϕ_{eff} [–] is the effective porosity, ϕ [–] is the total porosity and S_s [–] is the solid saturation (volume of solid phase divided by pore volume). Flow

properties that depend on saturation, such as capillary pressure and relative permeability of the mobile phases, are calculated on the basis of the effective porosity. Moreover, the reduction/increase in pore space associated with precipitation/dissolution reduces/increases the permeability of the medium. Laboratory-scale experiments have shown that the impact of porosity changes on formation permeability is very complex and depends among other factors on the overall reduction of porosity, the pores geometry and the distribution of precipitate within the pore space, which are different for different porous media (Vaughan 1987; Verma and Pruess 1988).

Third, phase equilibrium is affected by the presence of dissolved halite. Indeed, brine density, enthalpy, viscosity and vapor pressure (including vapor pressure lowering effects) depend on salinity (Battistelli et al. 1997; Pruess et al. 2011). Additionally, the solubility of non-saline components in the aqueous phase decreases with increasing salinity (salting out effect, or modification of Henry's constant not only as a function of temperature, but also salinity). The EWASG (WAter, Salt, Gas) EOS module of TOUGH2 (Battistelli et al. 1993; Pruess et al. 2011) effectively accounts for the thermodynamic properties of aqueous fluids of variable salinity. Recently, an improved version of this EOS was developed to overcome some limitations (Battistelli 2012). For instance, in the original version, the use of brine and halite correlations (for density, enthalpy and solubility) from different sources could lead to a lack of internal consistence. In the modified version, the work of Driesner (2007) and Driesner and Heinrich (2007) regarding brines and halite is implemented, and its use reduces potential internal inconsistencies.

In the simulations presented here, mass components are water, NaCl and air. The precipitate and the rock are the same substance (halite), and the liquid phase (brine) is always saturated with NaCl. In this scenario, halite solubility effects are included by increasing slightly the total initial porosity of the material (natural salt, crushed salt), and assigning an initial solid phase, so that the initial effective porosity (Eq. 1) is the target porosity. In order for EWASG to model the correct thermodynamic processes and phase equilibrium, some solid phase should always be present in each element of the mesh; this condition is satisfied in the simulations presented.

The temperature-dependent solubility of halite in the aqueous phase is modeled using the approach proposed by Driesner and Heinrich (2007). Regarding NaCl solubility in the gas phase, which is also temperature-dependent, we use Palliser and McKibbin's (1998) correlation. Figure 1 shows both solubilities (in terms of mass fraction) as a function of temperature. As it can be seen, the solubility in the gas phase is orders of magnitude smaller than in the aqueous phase. Note that any pressure dependence of halite

solubility is neglected in this study, as it is negligible for temperatures smaller than 400 °C (Driesner 2007).

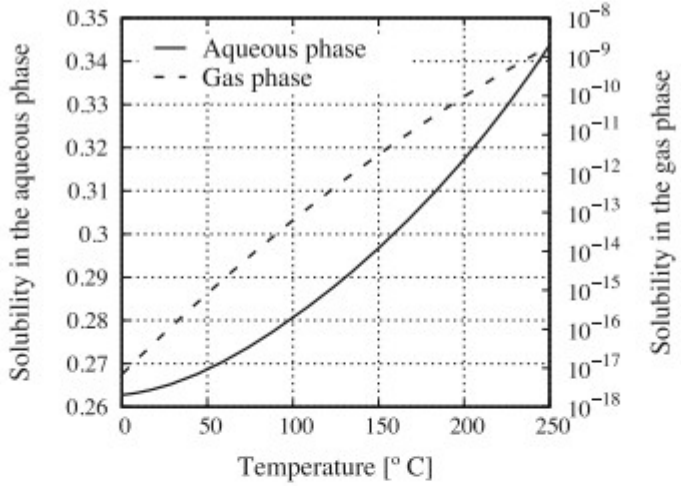

Fig. 1 Temperature-dependent solubility of halite (in terms of mass fraction) in the aqueous phase (left *y* axis) and in the gas phase (right *y* axis)

Fig. 2 Density of solid halite as a function of pressure and temperature in the relevant range for this research

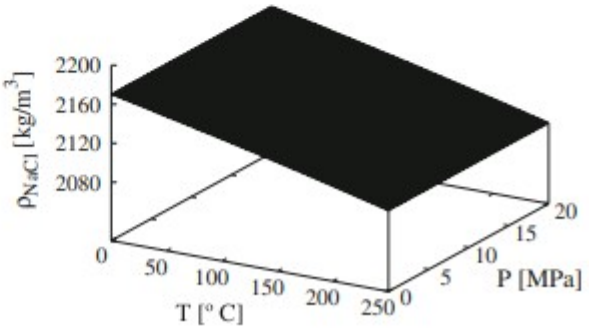

Brine viscosity follows the approach in Phillips et al. (1981). Regarding density and enthalpy of solid halite and brines of different salinity, we use the models presented in Driesner (2007); these models include temperature and pressure dependencies. Figure 2 displays the density of solid halite in the range of interest for this work; its analytical form is

2.2 TOUGH-FLAC Augmented with Halite Solubility Constraints

The simulator TOUGH-FLAC extended to the finite strain framework (Blanco-Martín et al. 2017) is used to perform the simulations presented. TOUGH-FLAC (Rutqvist et al. 2002; Rutqvist 2017) is a sequentially coupled simulator for coupled THM processes modeling. As the name suggests, TOUGH2 (Pruess et al. 2011) is used to solve the flow sub-problem (multicomponent, multiphase and nonisothermal), and FLAC^{3D} (Itasca 2012) is used to solve the geomechanics sub-problem (including time-dependent rheology). The flow sub-problem is solved first within a time-step, and relevant information is

passed between the two codes using the intermediate solution information technique (Settari and Mourits 1998). The coupling between the codes (two-way coupling) is based on the fixed-stress split sequential method (Kim et al. 2009). From flow to geomechanics, changes in pore pressure and temperature are used to compute a corrected stress tensor (Blanco-Martín et al. 2015a), and from geomechanics to flow the volumetric strain increment is used to compute a porosity correction term (Kim et al. 2012). Additionally, the new stress state at equilibrium is used to compute mechanically induced changes in flow properties. The coupling functions used for the natural salt and the crushed salt are fully detailed in Blanco-Martín et al. (2015a) and Rutqvist et al. (2002). The thermal conductivity of the natural salt decreases as temperature increases following

$$\lambda_{\text{salt}} = 5.734 - 1.838 \cdot 10^{-2} T + 2.86 \cdot 10^{-5} T^2 - 1.51 \cdot 10^{-8} T^3 \tag{3}$$

where λ_{salt} [W/m/K] and T [°C] (Bechthold et al. 1999). Regarding the crushed salt, its thermal conductivity increases during compaction following

$$\lambda_{\text{crushed salt}} = 5 + 1.5\phi_{\text{eff}} - 136\phi_{\text{eff}}^2 + 370\phi_{\text{eff}}^3 - 270\phi_{\text{eff}}^4 \tag{4}$$

with $\lambda_{\text{crushed salt}}$ [W/m/K] and ϕ_{eff} [–] (Bechthold et al. 2004). Note that Eq. (4) should be used only for $\phi_{\text{eff}} \leq 0.39$. In turn, the secondary permeability developed within the natural salt due to thermo-mechanical damage has the form

$$k_{\text{salt}}^{\text{secondary}} = 10^{\log\left(k_{\text{min}}^{\text{secondary}}\right) + \left\langle \log(\varepsilon_{vol}) - \log(\varepsilon_{vol,0}) + a_1 \exp(a_3 \sigma'_{\perp 2}) \frac{1}{\ln(10)} \left(\text{Ei}(a_2\, \varepsilon_{vol}) - \text{Ei}(a_2\, \varepsilon_{vol,0})\right) \right\rangle_{k^*}} \tag{5}$$

where $\langle x \rangle = (x + |x|)/2$, $k_{\text{min}}^{\text{secondary}}$ [m^2] is the minimum secondary permeability at the onset of thermo-mechanically induced damage (typically, 10^{-22} m^2 for domal salt), $\varepsilon_{vol} \geq 0$ [–] is the non-elastic volumetric strain, $\varepsilon_{vol,0}$ [–] is the volumetric strain at which $k_{\text{min}}^{\text{secondary}}$ starts to develop due to the connection of micro-fissures, $\sigma'_{\perp 2}$ [MPa] is the effective stress perpendicular to the orientation of the micro-fissures, Ei(x) is the exponential integral function, and $k^* = 1$ m^2 (Wolters et al. 2012). Parameters a_1 [–], a_2 [–] and a_3 [MPa^{-1}] are salt-specific. Equation (5) is also used to model the permeability recovery due to healing (dilatancy decrease). The secondary permeability developed due to fluid infiltration follows

$$k_{\text{salt}}^{\text{secondary}} = 10^{i_1 + i_2 \arctan(i_3 \Delta P_{FI}) + i_4 \exp(i_5 \Delta P_{FI})} k^* \quad (6)$$

where $\Delta P_{FI} = \sigma_3 + P \geq 0$ [MPa] (σ_3 is the least compressive principal stress and P is the pore pressure), $k^* = 1$ m^2 and i_1 [–], i_2 [–], i_3 [MPa^{-1}], i_4 [–] and i_5 [MPa^{-1}] are salt-specific parameters (Wolters et al. 2012). When $\Delta P_{FI} \approx 1$–2 MPa, opening of grain boundaries and/or micro-fractures occur, leading to fluid infiltration (Fokker 1995; Kenter et al. 1990; Popp and Minkley 2010).

With a view to the permeability changes mentioned above that arise from changes in the effective porosity induced by NaCl dissolution/precipitation, and that are material-dependent, little information could be found for rock salt. In a first stage, we have assumed that the relationship between permeability and active porosity follows a power law, similar to the relationship between porosity and permeability within the crushed salt during compaction (Bechthold et al. 2004):

$$k = 5.67959 \cdot 10^{-11} \phi_{eff}^{4.355} k^* \quad (7)$$

with k [m^2] ($k^* = 1$ m^2), which replaces $k_{\text{min}}^{\text{secondary}}$ in Eq. (5) and 10i110i1 k^* in Eq. (6). The use of this model implies that the precipitate creates around the pore walls, but there is no current evidence to confirm this assumption. Experimental work should be conducted to quantify permeability changes of natural salt induced by solubility changes, and the pertinence of Eq. (7) should be evaluated.

Finally, regarding the geomechanics sub-problem, the mechanical constitutive model used for the crushed salt has been modified to prevent the precipitate from compacting (i.e., only the effective porosity is subject to compaction).

3 Modeling of Laboratory and Field Data

In this section, we compare results from EWASG and TOUGH-FLAC with available experimental data of saliferous materials under thermal gradients. The target of this exercise is to evaluate whether our numerical tools are able to reproduce processes that will be relevant in the context of disposal of heat-generating nuclear waste in salt-based materials. The first case is related to a field test performed in natural salt at WIPP in the 1980s and involves THM coupling with TOUGH-FLAC. The last two cases are related to crushed salt and involve TH coupling, solved with TOUGH2.

3.1 Brine Release in a Field Test in Natural Salt

In order to improve quantitative predictions of brine movement, four brine migration tests were performed in rooms A1 and B of WIPP during the 1980s (Nowak 1986; Nowak and McTigue 1987), in boreholes prepared for the waste package performance technology experiments (Beraun and Molecke 1987). Several vertical boreholes were drilled in each room, and a metallic cylinder containing an electrical heater was placed in each borehole. In room A1, two brine migration tests were performed, in boreholes having 470 W electrical heaters that represent defense high-level waste at near-reference conditions. Conversely, in room B, the two brine migration tests were performed in boreholes having 1500 W electrical heaters that represent overtest conditions. The boreholes were instrumented to monitor strains at different depths. Prior to heating, the boreholes were left at ambient temperature for a few days. Brine inflow from the rock salt into the borehole was collected and measured periodically, both during the isothermal and the heating phases. For this, a nitrogen flow circulated in each borehole, transporting water vapor to a collection and measurement system outside the boreholes. The water released from each borehole was assumed to come from the brine that migrates from the salt rock mass toward the borehole. Since brine migration occurred during the isothermal phase and not only during heating, at rates higher than those predicted using models of inclusion migration, rather than the motion of intracrystalline inclusions under a temperature gradient, here another mechanism is dominant (McTigue and Nowak 1987). In particular, these experiments allow exploring (intergranular) Darcy flow in rock salt, resulting from the pore pressure gradient induced by the excavation and by differential thermal expansion effects between the rock mass and the intercrystalline fluid. However, the extent of this pressure gradient appears to be very limited around the boreholes (Nowak and McTigue 1987) and does not imply an unbounded domain of interconnected pore space.

Due to availability of more reliable data, we have studied test A1041 performed in room A1, in a borehole drilled approximately 6 months before the installation of the electrical heater. The borehole is 5.5 m long and has a diameter of 76 cm, and the waste container is 3 m long and has a diameter of 61 cm. In this room, which is 93.3 m long and has a cross-section of 5.5 m side, the boreholes are placed along the longitudinal axis in a single-row configuration. The central part of the room (about 41 m) is occupied with 1.41 kW guard heaters, 3.44 m apart. Close to each end of the room lie three boreholes containing 470 W canisters, spaced by 1.9 m between them and to the closest guard heater. The brine migration tests were performed in the two 470 W boreholes closest to the guard heaters. Figure 3 shows a schematic representation of test A1041, including the location of the instrumentation. Temperature and deformation were monitored during the

isothermal and the heating phases. Strains were calculated using relative displacements between two anchor points 20 cm apart.

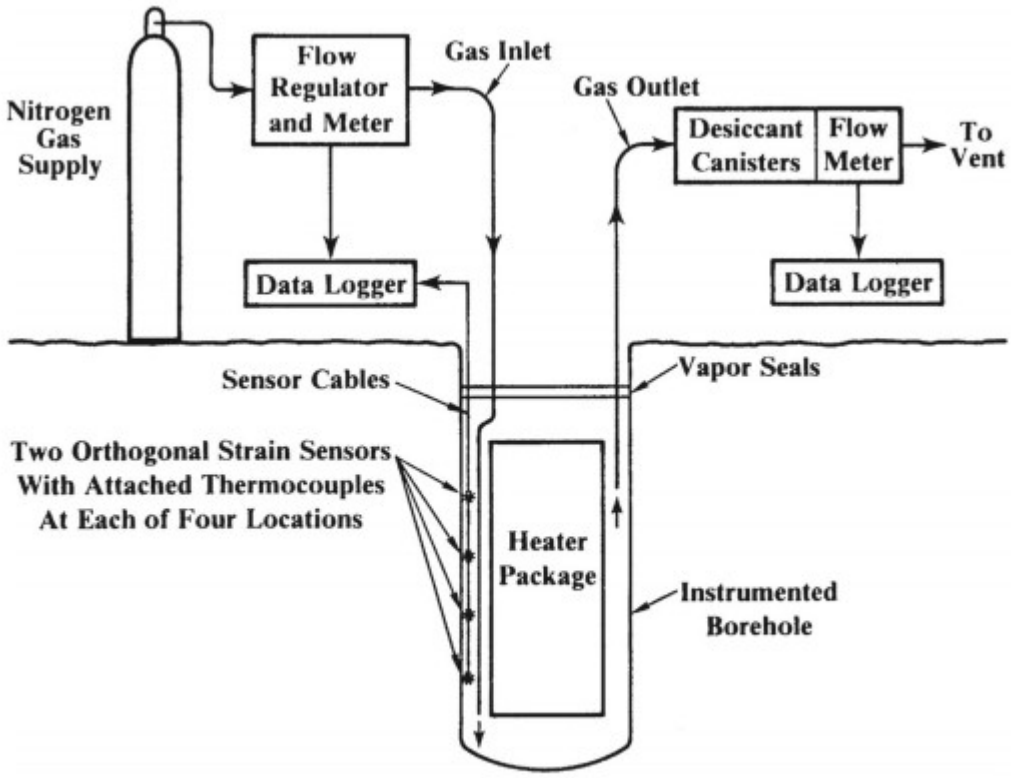

Fig. 3 Schematic view of WIPP test A1041 (after Nowak 1986). The borehole is sealed after emplacement of the electrical heater

The A1041 brine release experiment has been modeled with TOUGH-FLAC, using a three-dimensional domain of one quarter of the borehole and surrounding rock salt, reproducing the geometry shown in Fig. 3. Horizontally, the model extends 0.95 m along one axis (half distance between boreholes) and 11.75 m along the second axis (half distance to closest drift), and vertically, it extends 15 m to allow sufficient heat propagation without boundary effects. The simulation covers the six-month period prior to the installation of the heater, and the test itself (7.1 days before heater turn-on, and 154.9 days of heating); however, the analysis focuses on the phase after heater installation, since no measurements are available during the initial six-month period (this phase is modeled to compute an initial state for the subsequent 162 days). Table 1 lists the flow and mechanical properties of the rock salt. According to data in McTigue and Nowak (1987), the initial porosity of the surrounding rock salt has been estimated to be 0.5%, and the initial permeability to $5.4 \cdot 10^{-21}$ m^2 (Eq. (7)). Relative permeability and water retention properties are taken from Camphouse et al. (2012) and Jové-Colón et al. (2012). The thermal conductivity follows Eq. (3).

Table 1 THM modeling of test A1041 performed at WIPP: mechanical and flow properties of the natural salt host rock

Property (unit)	Value
Grain density, ρ_{grains} (kg/m^3)	2,164[a]
Bulk modulus, K (MPa)	20,600[b]
Shear modulus, G (MPa)	12,400[b]
Linear thermal expansion coeff., α_T (K^{-1})	$3.8 \cdot 10^{-5}$
Biot coefficient, α (–)	0.008[b]
Specific heat, C_0 (J/kg/K)	860
Relative permeability functions	Corey
Residual liquid saturation, S_{lr} (–)	0.1
Residual gas saturation, S_{gr} (–)	0
Van Genuchten's λ (–)	0.6
Van Genuchten's P_0 (MPa)	5.7[c]
Van Genuchten's S_{lr} (–)	0.01

[a]Equation (2); [b]damage- and healing-dependent value; [c]non-constant value (Leverett scaling)

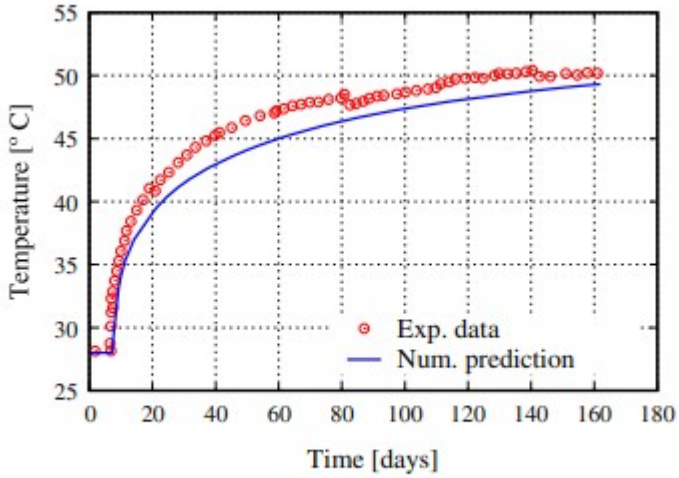

Fig. 4 WIPP test A1041: comparison between experimental data and numerical predictions for temperature at mid-heater height

The mechanical behavior of the host rock is modeled using the *Lux/Wolters* model (Wolters et al. 2012), in which the inelastic strain-rate tensor includes a damage-free creep component (nonlinear Burgers model with stationary and transient creep), a damage-induced component (dilatancy) and a sealing/healing component (reduction of dilatancy and damage). Initially, the stress state is isotropic and equal to − 14.8 MPa, and the pore pressure is hydrostatic, equal to 5.9 MPa. Although the initial pore pressure is probably between hydrostatic and lithostatic, we use the same value as in McTigue and Nowak (1987). The initial temperature is 28 °C. Figure 4 compares experimental and predicted temperatures at heater mid-height, and Fig. 5 compares experimental and predicted circumferential strains at the four locations displayed in Fig. 3. As it can be seen, temperature is slightly under

predicted, although the comparison is overall satisfactory. The modeled hoop strains increase rapidly once heating starts due to thermal effects; particularly, the thermal expansion coefficient used seems to be too high. We have used this value because it is typical for salt; nonetheless, and provided that the measurements are accurate, it could be that this coefficient is different in the current scenario due to local effects (impurities, intersecting layers, etc.). Note, however, that the strain rates beyond 20 days are captured quite well. The comparison between measured and predicted cumulative water collected from the borehole is plotted in Fig. 6a, and the corresponding inflow rates are shown in Fig. 6b. As heating starts, the experimental rate increases, which explains the steep slope shown in the cumulative water data. Thereafter, the rate decreases progressively and stabilizes (at about 8 g/day), yielding a constant slope in the cumulative data. Regarding the simulation results, the initial increase in the rate is not as high as the one measured, but the constant slope period is reproduced rather satisfactorily. Owing to the initial differences, the predicted amount of water collected is 1.5 kg, while the measured amount after 162 days is approximately 1.8 kg. Provided that the data are accurate, such differences could be related to the presence of intersecting layers with higher brine amounts (or higher permeability), or to thermal effects (e.g., expansivity, viscosity) not fully captured in the simulation.

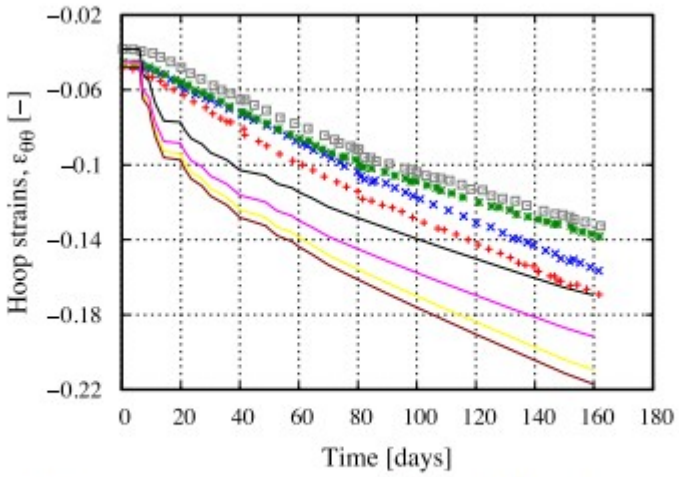

Fig. 5 WIPP test A1041: comparison between experimental data (symbols) and numerical predictions (lines) for hoop strains at the locations shown in Fig. 3 (* symbols). The strain values are relative to an arbitrary zero

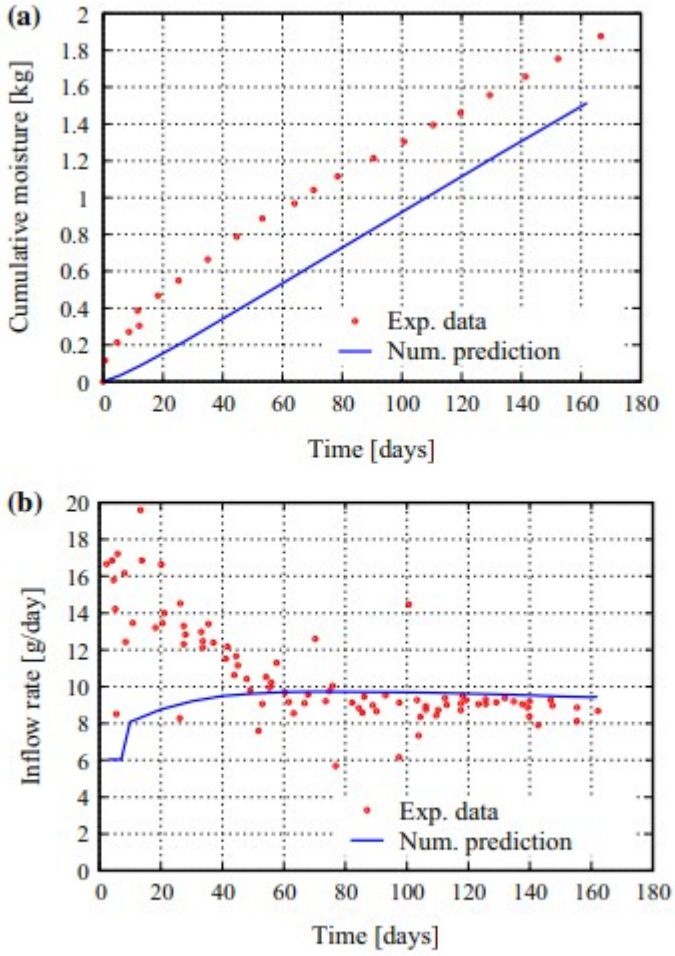

Fig. 6 WIPP test A1041: comparison between experimental data and numerical predictions for **a** cumulative water recovered from the borehole and **b** inflow rates

3.2 Porosity Variations in Crushed Salt

Olivella et al. (2011) present a series of experiments on granular salt (1–2 mm grain size). During each test, a temperature gradient is applied to a cylindrical sample having a length of 100 mm and a diameter of 50 mm. The system is closed, and therefore the mass remains constant. Moreover, axial deformation is blocked at the two ends of the sample. The temperature at one end is held at 85 °C, and it is held at 5 °C at the other end. The lateral surface of the sample is kept at adiabatic conditions. The temperature gradient between the two ends is maintained for 65 days. Olivella et al. (2011) performed several tests using different initial porosities: 20, 30 and 40%. Similarly, three values of initial liquid saturation were investigated: 10, 30 and 40%. For brevity, here we focus on the reference case established by the authors, namely initial porosity of 30% and initial saturation of 40%.

Due to the temperature gradient along the sample, there is a gradient of steam concentration in the gas phase that triggers mass transport (by diffusion) along the gradient direction. As steam condenses in cooler zones, a flow of the liquid phase toward the hot end of the sample is established, mainly governed by capillary forces, modified by the Leverett factor (see below). As the water evaporates close to the hot end, precipitation of dissolved NaCl occurs, which reduces the effective porosity. Similarly, as water vapor condenses at further distances from the hot end, dissolution of solid halite takes place, which increases the effective porosity. Modeling porosity changes due to halite solubility constraints is therefore an important aspect of this numerical exercise. The Olivella et al. (2011) experiments have been recently modeled by other authors (Bourret et al. 2016; Johnson et al. 2017).

A one-dimensional representation of the experiment is used, and mechanical effects are neglected. Flow parameters used to model this test are listed in Table 2. Since the grain size is quite different from typical values in nuclear waste disposal, rather than Eq. (7) we use $k = 1.89 \cdot 10^{-10} \phi_{eff}^{4.355} k^*$ to ensure that the initial permeability is 10^{-12} m^2 for $\phi_0 = 30\%$ (value provided by Olivella et al. 2011). Water retention properties are taken from the same reference, and during the simulation, the capillary pressure is scaled using the Leverett (1941) factor to account for the effect of porosity and permeability changes (see Eq. (21) in Rutqvist et al. 2002). The thermal conductivity is calculated using Eq. (4). As for diffusive transport, the diffusion coefficient of water in the gas phase depends on pressure and temperature (Pruess et al. 2011; Vargaftik 1975; Walker et al. 1981), and tortuosity is set to 0.4.

Table 2 TH modeling of experiments performed by Olivella et al. (2011) and Stauffer et al. (2013): flow properties of the crushed salt

Property (unit)	Value
Grain density, ρ_{grains} (kg/m^3)	2,164[a]
Specific heat, C_0 (J/kg/K)	860
Permeability, k_0 (m^2)	10^{-12}
Relative permeability functions	Corey
Residual liquid saturation, S_{lr} (–)	0.03
Residual gas saturation, S_{gr} (–)	0
Van Genuchten's λ (–)	0.6
Van Genuchten's P_0 (kPa)	1.6
Van Genuchten's S_{lr} (–)	0.02

[a]Equation (2)

Figure 7a, b compares our numerical predictions with available experimental data, and Fig. 7c shows the temperature gradient along the sample at the dates shown in Fig. 7a, b. It should be noted that the experimental data

contain inevitably some scatter, as different tests were performed at each of the dates shown (the samples were cut into slices to determine the porosity and the volumetric brine content [destructive technique]). The comparison is rather satisfactory, although there are some differences close to the cold end of the sample; these may be due to the fact that macro-voids are observed in some samples (see Fig. 4 in Olivella et al. 2011), due to steam condensation and halite dissolution (i.e., strong extraction of salt); consequently, using a continuum modeling approach may be inaccurate near the cold end of the sample. This was already highlighted by Olivella et al. (2011). Overall, the condensation front propagates from the hot end to the cold end during the experiment; this front is strongly related to the porosity peaks shown in Fig. 7a, which correspond to the greatest dissolution of NaCl. In turn, the volumetric brine content does not change significantly: close to the hot end, liquid saturation increases but porosity decreases due to NaCl precipitation as the water evaporates, and at further distances, the porosity increases due to NaCl dissolution (until saturation of the liquid phase), but the liquid saturation is small as the aqueous phase flows toward the hot end due to capillary forces, modified by the Leverett factor (in the hot end, porosity and therefore permeability decrease, and capillary forces increase).

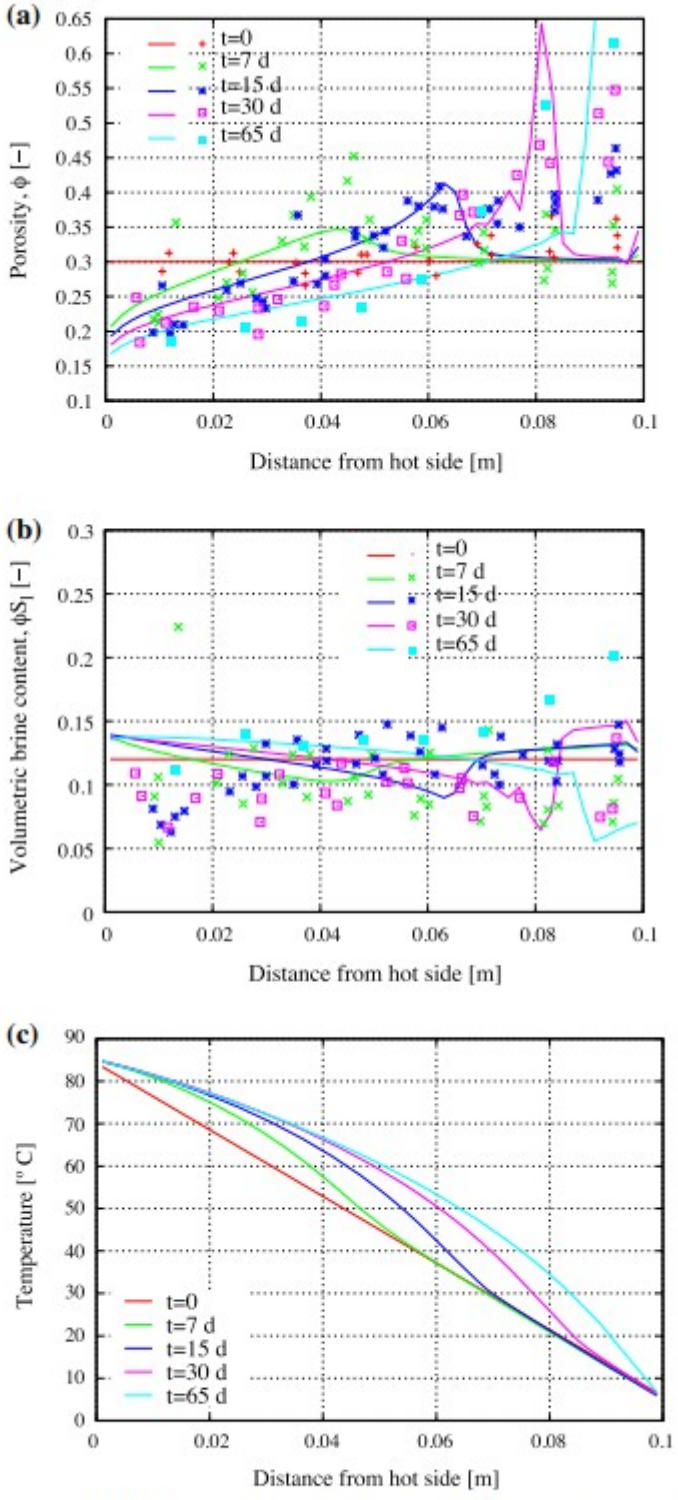

Fig. 7 Thermal test on crushed salt performed by Olivella et al. (2011): comparison between experimental data (symbols) and numerical predictions (lines) for **a** porosity and **b** volumetric brine content. **c** Computed evolution of temperature during the experiment

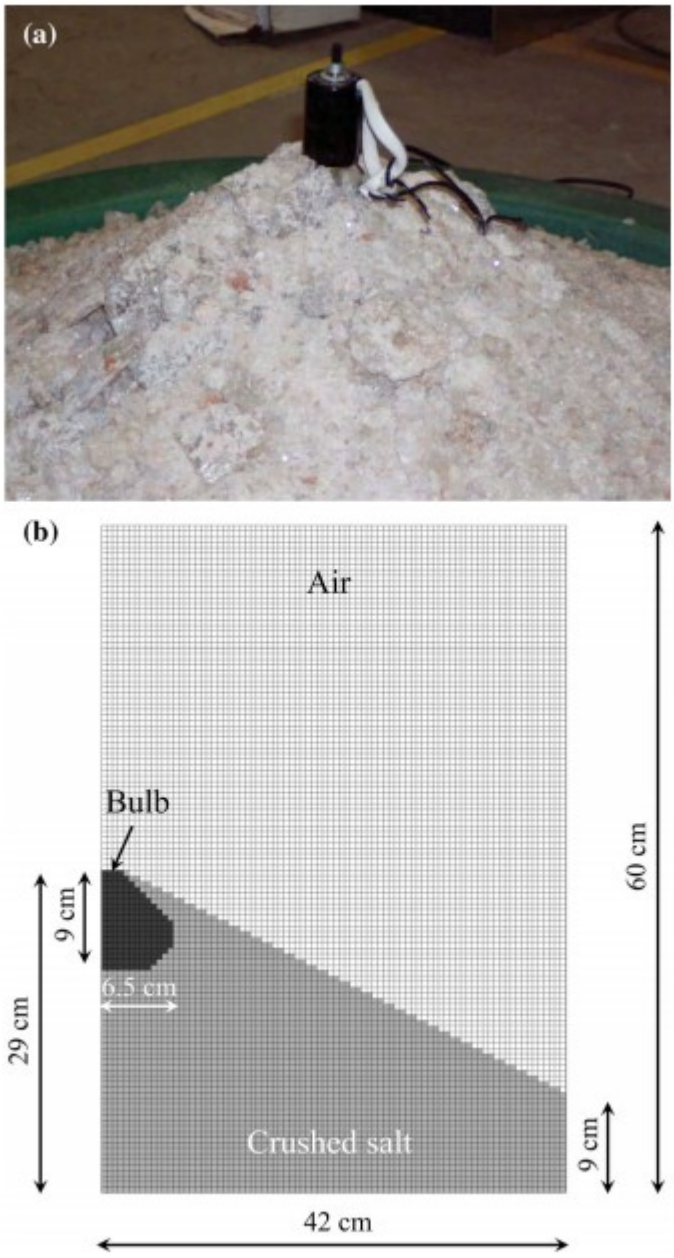

Fig. 8 Thermal test on a pile of crushed salt (Stauffer et al. 2013). **a** View of the experiment; **b** axisymmetric model prepared

3.3 Heat Propagation Through a Pile Cone of Crushed Salt

Stauffer et al. (2013) present experimental and modeling results of a thermal experiment conducted on crushed salt. In this experiment, a 125 W bulb is mostly submerged in crushed salt piled into a cone shape. Figure 8a shows a view of the crushed salt and the visible part of the bulb. The duration of the test is 2 h, and the initial temperature is 26 °C. The initial porosity of the crushed salt is 37.5%, and the initial liquid saturation is 1%. Temperatures are recorded at a frequency of 1 min, at two distances from the bottom of

the bulb: 6.35 and 15.2 cm. In this case, the focus is on modeling heat propagation within the pile of crushed salt (the saturation is small, and therefore porosity changes due to dissolution/precipitation are limited during the test). Although the test duration is very short compared to the time scales relevant for nuclear waste disposal, the data available can be compared with model predictions.

We have modeled this experiment in axisymmetric conditions (see Fig. 8b), neglecting mechanical effects. The parameters used are listed in Table 2, with the residual liquid saturation set to $S_{lr} = 0.1$. The comparison between measured and predicted temperatures at 6.35 and 15.2 cm below the bulb are displayed in Fig. 9 (for the position 6.35 cm, we have plotted predictions at 6 and 6.5 cm because the mesh resolution is 5 mm). As the figure shows, the agreement is quite good.

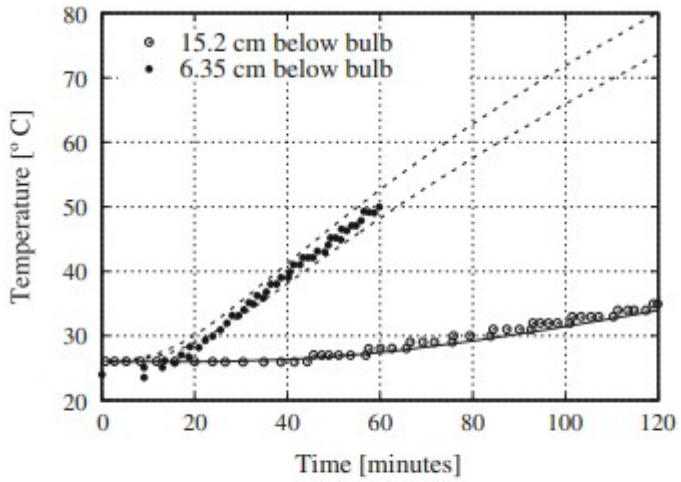

Fig. 9 Thermal test on a pile of crushed salt (Stauffer et al. 2013): comparison between experimental data (symbols) and numerical predictions (lines) for temperature at two locations below the bulb. For the location 6.35 cm below the bulb, results at the two nearest nodes are displayed

4 Long-Term Modeling of a Generic Salt Repository for Heat-Generating Nuclear Waste

In this section, a generic salt repository for heat-generating nuclear waste is modeled over a time period of 100,000 years. In order to evaluate the effects of halite solubility constraints on the numerical predictions, two THM simulations are performed: one includes those constraints, and the other disregards them. The former is considered as the reference scenario, and results of the latter are only discussed if they present features or significant differences as compared to the reference case. To conduct the simulations, we use the TOUGH-FLAC simulator described in Sect. 2.

The model geometry and heat load are similar to those used in previous studies (Blanco-Martín et al. 2015a, b, c). Figure 10 shows an overview of the model geometry and an enlarged view of the drift area. The model extends 1200 m along the *Z*-axis and 25 m along the *X*-axis to account for typical drift spacing of 50 m. Plane strain conditions are assumed. A 400-m-thick salt layer is confined between two sandstone layers, also 400 m thick. The repository emplacement drift is located at a depth of 600 m and is 4.5 m wide and 3.5 m high. The waste packages have a diameter of 1.6 m and are placed parallel to the drift axis. The remaining space between the packages and the drift wall is backfilled with crushed salt, having an initial porosity of 35%.

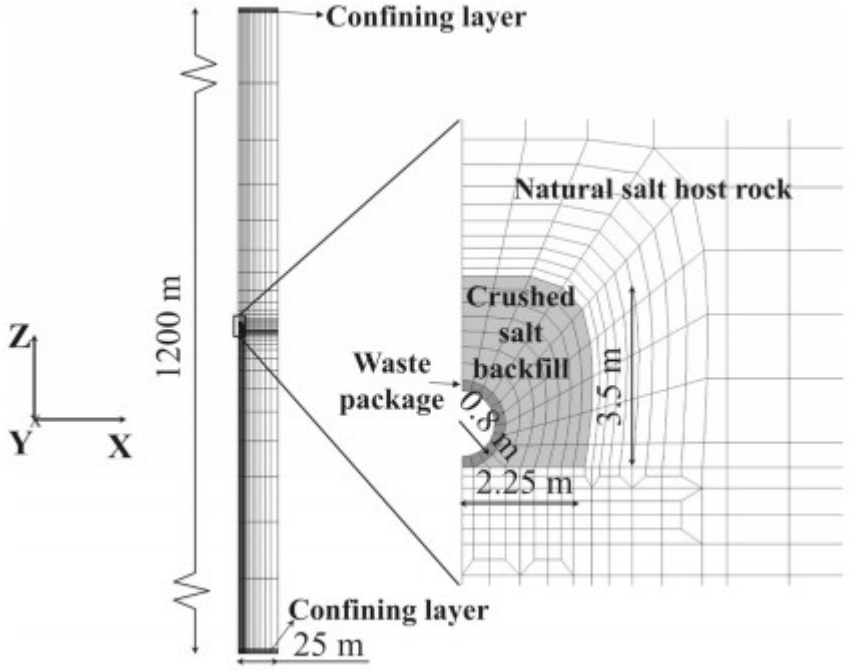

Fig. 10 Geometry of the generic salt repository considered and enlarged view of the drift area

In the flow sub-problem, mass flow occurs by advection and diffusion, and heat transport occurs by conduction and convection. The mechanical response of the natural salt is modeled using the *Lux/Wolters* constitutive model (Wolters et al. 2012). The mechanical behavior of the crushed salt is ruled by a modified version of the *cwipp* model implemented in FLAC^{3D}, in which the strain-rate tensor comprises a nonlinear elastic component, a viscous compaction component and a purely deviatoric viscous term (Itasca 2012). As compaction takes place, density increases toward that of the natural salt at a rate derived from experimental results. During this process, the shear and bulk moduli increase in an exponential fashion. While density is not allowed to decrease in the *cwipp* model, it honors the volumetric strain

evolution in our modified version. Moreover, as explained in Sect. 2.2, in the current investigation only the pore space occupied by mobile fluids is subject to compaction. The confining layers and waste packages are assumed to behave elastically. Table 3 lists flow and mechanical properties of the crushed salt, the natural salt and the confining layers. The parameters used for natural salt and crushed salt are based as much as possible on available data (Bechthold et al. 1999, 2004; Camphouse et al. 2012; Jové-Colón et al. 2012; Olivella et al. 2011); these properties evolve as detailed in Sect. 2 and Blanco-Martín et al. (2015a). Tortuosity is assumed equal to the relative permeability of each phase, and the diffusion coefficient (water in the gas phase) is pressure and temperature dependent (Pruess et al. 2011; Vargaftik 1975; Walker et al. 1981). Regarding the mechanical response of the crushed salt, the parameters needed to model compaction have been recently calibrated, as have been three parameters that control the stationary creep of the natural salt (Blanco-Martín et al. 2016).

Table 3 THM modeling of a generic salt repository: mechanical and flow properties of the crushed salt, the natural salt and the confining layers

Property (unit)	Crushed salt	Rock salt	Confining rock
Grain density, ρ_{grains} (kg/m^3)	2,164[a]	2,164[a]	2600
Bulk modulus, K (MPa)	7.3[b]	17,390[c]	37,900
Shear modulus, G (MPa)	4.0[b]	9,450[c]	19,500
Linear thermal expansion coeff., α_T (K^{-1})	$3.8{\cdot}10^{-5}$	$3.8{\cdot}10^{-5}$	10^{-5}
Biot coefficient, α (–)	1[b]	0.003[c]	1
Relative permeability functions	Corey	Corey	Van Genuchten (liquid), Corey (gas)
Residual liquid saturation, S_{lr} (–)	0.1	0.1	0.02
Residual gas saturation, S_{gr} (–)	0	0	0.01
Van Genuchten's λ (–)	0.6	0.6	0.6
Van Genuchten's P_0 (MPa)	0.0003[d]	5.7[d]	3.6
Van Genuchten's S_{lr} (–)	0.01	0.01	0.01
Effective liquid saturation, $S_{l,eff,0}$ (–)	0.02	1	1
Effective porosity, $\phi_{eff,0}$ (–)	0.35	0.002	0.12
Permeability, k_0 (m^2)	$5.87{\cdot}10^{-13}$	10^{-22}	10^{-12} [e]
Specific heat, C_0 (J/kg/K)	860	860	900[e]
Thermal conductivity, λ_0 (W/m/K)	0.68	5.24	1.8[e]

[a]Equation (2); [b]non-constant value (changes during reconsolidation); [c]damage- and healing-dependent value; [d]non-constant value (Leverett scaling); [e]constant values (properties do not evolve due to THM coupling)

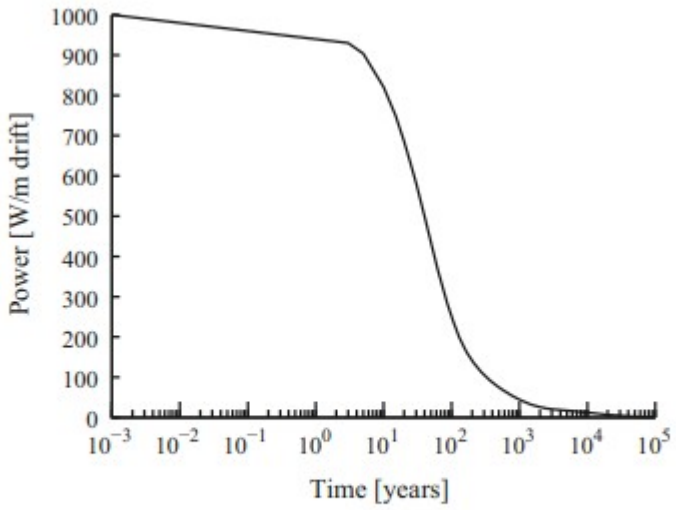

Fig. 11 Generic salt repository: heat load per meter of drift for a waste package containing 10 pressurized water reactor (PWR) assemblies, assuming underground emplacement after 20 years of interim storage. The waste packages are assumed to be 5.5 m long and spaced by 3 m along the drift axis

The initial stress state is isotropic and equals the lithostatic stress magnitude. The initial temperature follows a geothermal gradient of 0.025 °C/m, and the temperature at the ground surface is 10 °C. The initial pore pressure is hydrostatic, similarly to the modeling of the brine release experiment presented in Sect. 3.1. As for the boundary conditions, the displacement is restricted normal to the lateral and bottom boundaries, while the displacement at the top is not constrained. No flow is allowed across the lateral boundaries, and Dirichlet boundary conditions are imposed at the top and bottom.

The simulations comprise the following phases: initial equilibrium, drift excavation, emplacement of the waste packages and backfilling, and 100,000 years of post-closure. THM modeling is performed for the post-closure phase, after activation of the waste package and the backfill. Modeling the excavation of the drift (assumed instantaneous) induces changes in the stress state and the pore pressure within the host rock; the pore pressure obtained after excavation is exported to TOUGH2 to ensure that the initial conditions of the THM run are the same in the two codes. At emplacement, the crushed salt backfill and the waste package are at atmospheric pressure and 28 °C. The heat load applied during post-closure is displayed in Fig. 11 and is consistent with the expected nuclear waste characteristics within the US Department of Energy Spent Fuel and Waste Disposition Campaign (Carter et al. 2011).

Figure 12 displays the temperature evolution at several locations in the repository. Temperature peaks at about 220 °C in the waste package after one year. This value is slightly higher than that predicted previously (Blanco-

Martín et al. 2015a, b) due to the higher initial porosity of the crushed salt used here (35% instead of 30%); indeed, crushed salt thermal conductivity is lower for higher porosities (Eq. 4). As the backfill compacts over time, its thermal conductivity increases and heat propagates further in the host rock. After 100,000 years, temperature throughout the model has decreased to its initial value.

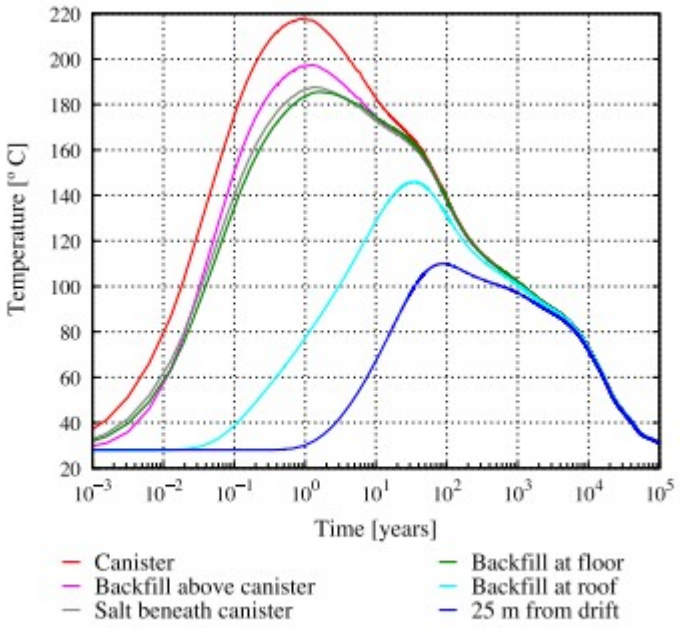

Fig. 12 Generic salt repository: evolution of temperature at several locations (post-closure phase)

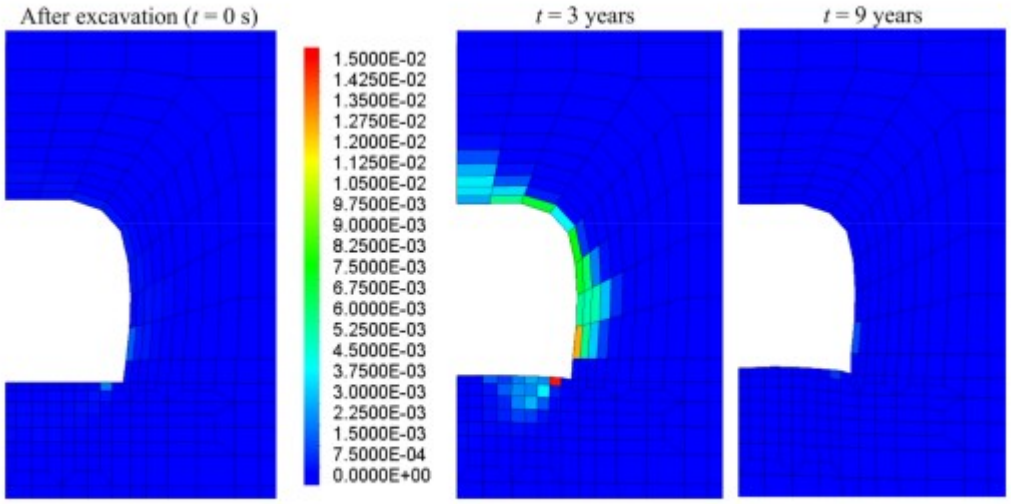

Fig. 13 Generic salt repository: extension of the EDZ (in terms of non-elastic volumetric strains) at three different moments of the post-closure phase

Compaction of the crushed salt is mainly triggered by the drift closure, which in turn is mostly induced by the creep of the natural salt host rock under the

effect of deviatoric stresses and temperature. As the backfill stiffens, an internal support is provided at the drift walls and the deviatoric stresses within the host rock decrease progressively, so that healing processes can be activated. Figure 13 shows the evolution of inelastic volumetric strains in the short-term. The dilatancy occurring during the first years brings about thermo-mechanical damage and the development of secondary permeability and porosity. After 3 years, the damaged zone extends about 1.1–1.4 m around the drift. However, as healing develops (due to the decrease in deviatoric stresses and the evolution toward a favorable stress state), the dilatancy created during excavation and the first years of post-closure is neutralized, and after about 8–9 years the initial tightness of the host rock is restored.

Figure 14 shows the evolution of the average crushed salt porosity in a cross-section. Compaction is not uniform in space, and starts above the waste package, at the corners and close to the drift roof. Note that as time moves forward, the responses of the *cwipp* and the *Lux/Wolters* models converge (the deviatoric stresses decrease in the host rock [damage is reversed by healing] and the elastic parameters of the crushed salt evolve toward those of the natural salt). As it can be seen, after about 100 years porosity is on average lower than 2.5%, and it reaches around 0.3% after 20,000 years (the assumed undisturbed porosity of natural salt is 0.2%, see Table 3). These results have been obtained using parameters of crushed salt compaction calibrated on the TSDE experiment, and predict significantly longer reconsolidation times than in previous investigations (about 20 years, see Blanco-Martín et al. 2015a). We highlight however that these results are not conclusive, as the reconsolidation of crushed salt at high temperatures needs to be further investigated, experimentally, theoretically and numerically. In any case, in the scenario studied mechanical compaction dominates over dissolution/precipitation of NaCl in the evolution of porosity. Figure 15 compares the porosity profile at different dates in the two cases investigated. Only minor differences can be seen, which suggest that mechanical effects dominate. At early times, evaporation of the water present creates a ring of NaCl precipitation near the waste package (radius of 0.6–0.7 m), and a dissolution ring is formed coincident with the ring of condensation, in a zone with lower temperature further from the waste package (upper row in Fig. 15). At later times, as temperature decreases throughout the repository (see Fig. 12), the solubility decreases and some NaCl precipitation occurs when dissolution/precipitation is accounted for, resulting in a slightly smaller porosity than in the no-solubility case. Nevertheless, given the small amount of brine present in the crushed salt (Table 3), the distribution of porosity is not significantly affected by dissolution/precipitation, and mechanical effects dominate. In general, the

initial liquid saturation of the crushed salt is small, and therefore, unless the content of impurities (which often act as hydrous sources) is high, the porosity profile will not be significantly affected by dissolution/precipitation. Since here we study a generic (i.e., not site-specific) repository, we have chosen a typical value of initial saturation for the crushed salt backfill.

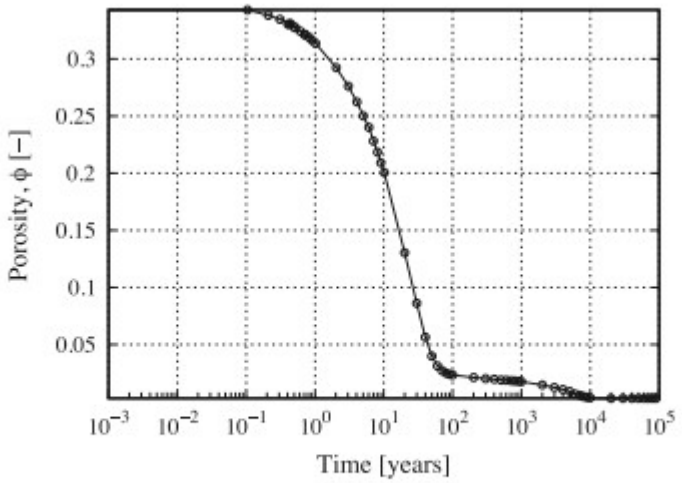

Fig. 14 Generic salt repository: evolution of crushed salt porosity (average value in a cross section of the drift) during the post-closure phase

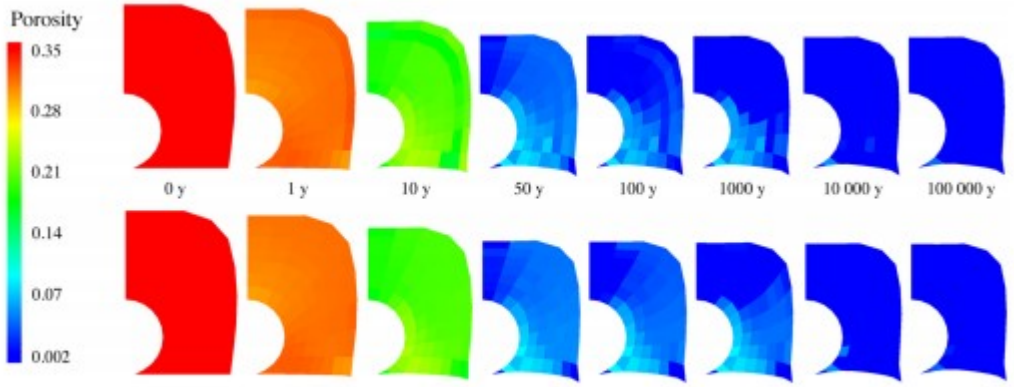

Fig. 15 Generic salt repository: crushed salt porosity at different dates during the post-closure phase. Top: case including halite solubility constraints; bottom: case neglecting halite solubility constraints

Figure 16 displays the evolution of pore pressure at several locations in the repository. In the host rock in the drift area, the initial value is smaller than hydrostatic due to the pore pressure decrease during the drift excavation. The pore pressure rise observed 25 m from the drift at about 10 years is due to thermal pressurization, developed as heat propagates (high thermal expansion of the pore fluids, which cannot escape in a very low permeability rock mass). In the drift area, the pore pressure rise observed between 10 and 100 years is mainly due to the porosity (and permeability) reduction in the crushed salt during reconsolidation, compare Figs. 14 and 16. As it can

be seen, the pore pressure peaks below 16 MPa, which suggests fluid infiltration occurs (opening of grain boundaries and/or micro-fractures since $\Delta P_{FI} \approx 1$–2 MPa). Pore pressure cannot increase much above the infiltration criterion ($\Delta P_{FI} = \sigma_3 + P \geq 0$) because infiltration (Eq. 6) will work against further pore pressure increase, and it cannot decrease below the infiltration criterion because the infiltration-induced grain boundary openings and/or micro-fractures will close again, triggering a new pore pressure increase, which will result in infiltration. Since the main cause to fluid permeation is the thermal pressurization of the pore fluid induced by the time-dependent heat load, as such load decreases both temperature and pore pressure decrease (see Figs. 12, 16). The area affected by fluid permeation reaches a maximum after about 300 years, and is significantly larger than the area affected by thermo-mechanical damage (which does not extend too far from the drift walls, see Fig. 13), but it does not reach the confining layers. After 100,000 years, the hydrostatic pore pressure is restored as shown in Fig. 16. Owing to the solubility increase with temperature at early times (see Fig. 1 and 12), there is an increase in the effective porosity and permeability as explained in part 2, which yields slightly less infiltration when halite solubility constraints are considered than when they are disregarded, but the overall processes and trends remain the same, both at early and later times. In this generic study, we have assumed that the changes in permeability of rock salt induced by dissolution/precipitation of halite follow Eq. (7); however, no experimental evidence supports this assumption, and additional experimental and numerical studies should be conducted before the predictions shown in this section can be validated.

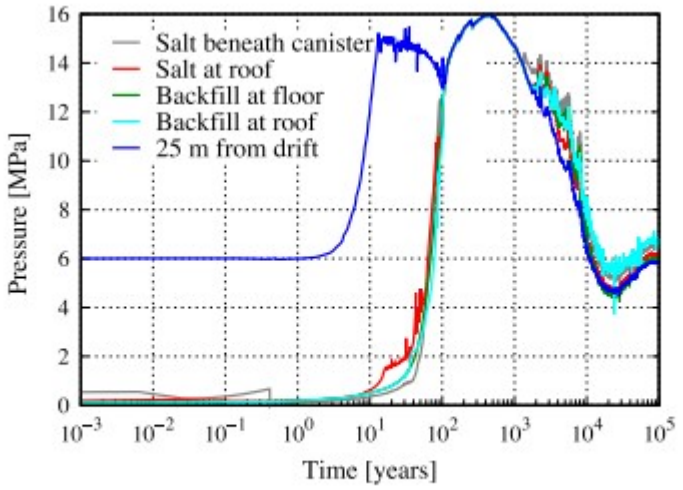

Fig. 16 Generic salt repository: evolution of pore pressure at several locations (post-closure phase)

5 Summary and Conclusions

In the context of disposal of heat-generating nuclear waste in salt-based formations, this paper presents numerical modeling of coupled thermal, hydraulic and mechanical processes in rock salt and crushed salt including halite solubility constraints. Although some experimental and modeling work is reported in the literature, the time scales considered are short, and to the best of the authors' knowledge the long-term performance at the repository scale has not yet been investigated including dissolution/precipitation effects. The TOUGH-FLAC simulator for coupled processes modeling has been adapted to account for halite solubility constraints.

The enhanced simulator is first applied to model available laboratory and field scale tests performed in rock salt and crushed salt, yielding overall satisfactory results. Then, it is applied to model the long-term response (100,000 years) of a generic salt repository for heat-generating nuclear waste. The effects of halite dissolution/precipitation are evaluated through the comparison of two simulations that, respectively, consider or neglect such effects. In the scenario considered, the results are not significantly affected by dissolution/precipitation, and only some differences are observed due to changes in porosity, but the dominating processes remain the same: mechanical compaction within the backfill, and thermo-mechanical damage, fluid permeation and healing within the host rock. We note however that these results are based on assumptions that need to be further investigated and validated experimentally and numerically, such as the evolution of permeability induced by halite dissolution/precipitation.

Overall, with the new provisions presented, TOUGH-FLAC is more complete in terms of processes occurring around a heat-releasing nuclear waste package and can therefore provide more accurate predictions of the long-term performance of a nuclear waste repository in salt formations.

Acknowledgements

Funding for this work has been provided by the Spent Fuel and Waste Disposition Campaign, Office of Nuclear Energy of the U.S. Department of Energy, under Contract Number DE-AC02-05CH11231 with Berkeley Lab.

References

Battistelli, A., Calore, C., Pruess, K.: A fluid property module for the TOUGH2 simulator for saline brines with non-condensible gas. In: Proceedings of 18th Workshop Geothermal Reservoir Engineering, Stanford, CA, pp. 249–259 (1993)

Battistelli, A., Calore, C., Pruess, K.: The simulator TOUGH2/EWASG for modelling geothermal reservoirs with brines and a non-condensible gas.

Geothermics 26(4), 437–464 (1997). https://doi.org/10.1016/S0375-6505(97)00007-2

Battistelli, A.: Improving the treatment of saline brines in EWASG for the simulation of hydrothermal systems. In: Proceedings of TOUGH Symposium, Berkeley, CA (2012)

Bechthold, W., Rothfuchs, T., Poley, A., Ghoreychi, M., Heusermann, S., Gens, A. et al.: Backfilling and sealing of underground repositories for radioactive waste in salt (BAMBUS Proj.). European Atomic Energy Community. Rep. EUR19124 EN (1999)

Bechthold, W., Smailos, E., Heusermann, S., Bollingerfehr, W., Bazargan Sabet, B., Rothfuchs, T.: Backfilling and sealing of underground repositories for radioactive waste in salt (BAMBUS II Proj.). European Atomic Energy Community. Rep. EUR20621 EN (2004)

Beraun, R., Molecke, M.A.: Thermal analysis of the WIPP in situ room A1 DHLW package experiments. SNL. Rep. SAND86-0681 (1987)

Bérest, P., Bergues, J., Brouard, B., Durup, G., Guerber, B.: A measurement of creep and permeability of a salt cavern (Une mesure de la perméabilité et du fluage d’une caverne dans le sel). Compte Rendu Académie des Sciences (Paris) 329, 103–108 (1999)

Blanco-Martín, L., Rutqvist, J., Birkholzer, J.T.: Long-term modeling of the thermal-hydraulic-mechanical response of a generic salt repository for heat-generating nuclear waste. Eng. Geol. 193, 198–211 (2015a). https://doi.org/10.1016/j.enggeo.2015.04.014

Blanco-Martín, L., Wolters, R., Rutqvist, J., Lux, K.-H., Birkholzer, J.T.: Comparison of two simulators to investigate thermal-hydraulic-mechanical processes related to nuclear waste isolation in saliferous formations. Comput. Geotech. 66, 219–229 (2015b). https://doi.org/10.1016/j.compgeo.2015.01.021

Blanco-Martín, L., Rutqvist, J., Birkholzer, J.T., Battistelli, A.: Long-term modeling of coupled processes in a generic salt repository for heat-generating nuclear waste: preliminary analysis of the impacts of halite dissolution and precipitation. In: Proceedings of 49th US Rock Mechanics/Geomechanics Symposium, San Francisco, CA. Paper ARMA 15-440 (2015c)

Blanco-Martín, L., Wolters, R., Rutqvist, J., Lux, K.-H., Birkholzer, J.T.: Thermal-hydraulic-mechanical modeling of a large-scale heater test to investigate rock salt and crushed salt behavior under repository conditions

for heat-generating nuclear waste. Comput. Geotech. 77, 120–133 (2016). https://doi.org/10.1016/j.compgeo.2016.04.008

Blanco-Martín, L., Rutqvist, J., Birkholzer, J.T.: Extension of TOUGH-FLAC to the finite strain framework. Comput. Geosci. 108, 64–71 (2017). https://doi.org/10.1016/j.cageo.2016.10.015

Bourret, S.M., Stauffer, P.H., Weaver, D.J., Caporuscio, F.A., Otto, S., Boukhalfa, H., Jordan, A.B., Chu, S., Zyvoloski, G.A., Johnson, P.J.: Experiments and modeling in support of generic salt repository science. LANL. Rep. LANL FCRD-UFD-2016-000445 (2016)

Broome, S.T., Bauer, S.J., Hansen, F.D.: Reconsolidation of crushed salt to 250°C under hydrostatic and shear stress conditions. In: Proceedings of 48th US Rock Mechanics/Geomechanics Symposium, Minneapolis, MN. Paper ARMA 14-7088 (2014)

Callahan, G.D., Mellegard, K.D., Hansen, F.D.: Constitutive behavior of reconsolidating crushed salt. RE/SPEC Inc. Rep. SAND-98-0179C (1998)

Camphouse, R.C., Gross, M., Herrick, C.G., Kicker, D.C., Thompson, B.: Recommendations and justifications of parameter values for the run-of-mine salt panel closure system design modeled in the PCS- 2012 PA. SNL. Final memo 5412 (2012)

Carter, J.T., Luptak, A.J., Gastelum, J., Stockman, C., Miller, A.: Fuel cycle potential waste inventory for disposition. SRNL. Rep. FCR&D-USED-2010-000031 Rev. 5 (2011)

Driesner, T., Heinrich, C.H.: The system H2O-NaCl. Part I: correlation formulae for phase relations in temperature-pressure-composition space from 0 to 1000 °C, 0 to 5000 bar, and 0 to 1 XNaCl. Geochim. Cosmochim. Acta 71, 4880–4901 (2007). https://doi.org/10.1016/j.gca.2006.01.033

Driesner, T.: The system H_2O-NaCl. Part II: Correlations for molar volume, enthalpy, and isobaric heat capacity from 0 to 1000°C, 1 to 5000 bar, and 0 to 1 X_{NaCl}. Geochim. Cosmochim. Acta 71, 4902–4919 (2007). https://doi.org/10.1016/j.gca.2007.05.026

Fokker, P.A.: The behaviour of salt and salt caverns. Ph.D. dissertation, TU Delft (1995)

Hardin, E., Voegele, M.: Alternative concepts for direct disposal of dual-purpose canisters. SNL. Rep. FCRD-UFD-2013-000102 Rev. (2013)

Hou, Z.: Mechanical and hydraulic behaviour of rock salt in the excavation disturbed zone around underground facilities. Int. J. Rock Mech. Min. Sci. 40, 725–738 (2003). https://doi.org/10.1016/S1365-1609(03)00064-9

Hunsche, U., Hampel, A.: Rock salt—the mechanical properties of the host rock material for a radioactive waste repository. Eng. Geol. 52, 271–291 (1999). https://doi.org/10.1016/S0013-7952(99)00011-3

Hurtado, L.D., Knowles, M.K., Kelley, V.A., Jones, T.L., Ogintz, J.B., Pfeifle, T.W.: WIPP shaft seal system parameters recommended to support compliance calculations. SNL. Rep. SAND-97-1287 (1997)

Itasca: FLAC^{3D} (Fast Lagrangian analysis of continua in 3 dimensions), Version 5.0. Itasca Consulting Group, Minneapolis, MN (2012)

Johnson, P.J., Bourret, S.M., Zyvoloski, G.A., Boukhalfa, H., Stauffer, P.H., Weaver, D.J.: Experiments and modeling to support field test design. LANL. Rep. LA-UR-17-27759 DMS SFWD-SFWST-2017-000102 (2017)

Jordan, A.B., Boukhalfa, H., Caporuscio, F.A., Robinson, B.A., Stauffer, P.H.: Hydrous mineral dehydration around heat-generating nuclear waste in bedded salt formations. Environ. Sci. Technol. 49(11), 6783–6790 (2015). https://doi.org/10.1021/acs.est.5b01002

Jové-Colón, C., Greathouse, J.A., Teich-McGoldrick, S., Cygan, R.T., Hadgu, T., Bean, J.E., Martínez, M.J., Hopkins, P.L., Argüello, J.G. Hansen, F.D.: Evaluation of generic EBS design concepts and process models: implications to EBS design optimization. SNL. Rep. FCRD-USED-2012-000140 (2012)

Kenter, C.J., Doig, S.J., Rogaar, H.P., Fokker, P.A., Davies, D.R.: Diffusion of brine through rock salt of roof caverns. In: Proceedings of SMRI Fall Meeting Paris (1990)

Kim, J., Tchelepi, H., Juanes, R.: Stability, accuracy and efficiency of sequential methods for coupled flow and geomechanics. In: SPE Reservoir Simulation Symposium (2009)

Kim, J., Sonnenthal, E.L., Rutqvist, J.: Formulation and sequential numerical algorithms of coupled fluid/heat flow and geomechanics for multiple porosity materials. Int. J. Numer. Meth. Eng. 92(5), 425–456 (2012). https://doi.org/10.1002/nme.4340

Korthaus, E.: Experiments on crushed salt consolidation with true triaxial testing device as a contribution to an EC benchmark exercise. Forschungszentrum Karlsruhe GmbH. Rep. FZKA-6181 (1998)

Kröhn, K.-P., Zhang, C.-L., Czaikowski, O., Stührenberg, D., Heemann, U.: The compaction behaviour of salt backfill as a THM-process. In: Proceedings of 8th Conference on Mechanical Behavior Salt (SaltMech8), pp. 49–59 (2015)

Leverett, M.C.: Capillary behaviour in porous solids. Petrol. Trans. AIME 192, 152–169 (1941)

McTigue, D.F., Nowak, E.J.: Brine transport studies in the bedded salt of the Waste Isolation Pilot Plant (WIPP). In: Proceedings of Fall Meeting Materials Research Society, Boston, MA (1987)

Nowak, E.J.: Preliminary results of brine migration studies in the Waste Isolation Pilot Plant (WIPP). SNL. Rep. SAND86-0720 (1986)

Nowak, E.J., McTigue, D.F.: Interim results of brine transport studies in the Waste Isolation Pilot Plant (WIPP). SNL. Rep. SAND87-0880 (1987)

Olivella, S., Castagna, S., Alonso, E.E., Lloret, A.: Porosity variations in saline media induced by temperature gradients: experimental evidences and modelling. Transp. Porous Med. 90, 763–777 (2011). https://doi.org/10.1007/s11242-011-9814-x

Palliser, C., McKibbin, R.: A model for deep geothermal brines, I: *T-P-X* state-space description. Transp. Porous Med. 33, 65–80 (1998). https://doi.org/10.1023/A:1006537425101

Phillips, S.L., Igbene, A., Fair, J.A., Ozbek, H., Tavanam, M.: A technical databook for geothermal energy utilization. LBNL. Rep. LBL-12810 (1981)

Popp, T., Kern, H., Schulze, O.: Evolution of dilatancy and permeability in rock salt during hydrostatic compaction and triaxial deformation. J. Geophys. Res. 106(B3), 4061–4078 (2001). https://doi.org/10.1029/2000JB900381

Popp, T., Minkley, W.: Salt barrier integrity during gas pressure build-up in a radioactive waste repository—implications from lab and field investigations. In: Proceedings of 44th US Rock Mechanics/Geomechanics Symposium, Salt Lake City, UT. Paper ARMA 10-493 (2010)

Pruess, K., Oldenburg, C.M., Moridis, G.: TOUGH2 user’s guide, version 2. LBNL. Rep. LBNL-43134 (rev.) (2011)

Pudewills, A., Droste, J.: Numerical modeling of the thermomechanical behavior of a large-scale underground experiment. Comput. Struct. 81, 911–918 (2003). https://doi.org/10.1016/S0045-7949(02)00427-3

Rege, S.D., Fogler, H.S.: Competition among flow, dissolution and precipitation in porous media. AIChE J. 35(7), 1177–1185 (1989). https://doi.org/10.1002/aic.690350713

Rutqvist, J., Wu, Y.S., Tsang, C.-F., Bodvarsson, G.: A modeling approach for analysis of coupled multiphase fluid flow, heat transfer, and deformation in fractured porous rock. Int. J. Rock Mech. Min. Sci. 39, 429–442 (2002). https://doi.org/10.1016/S1365-1609(02)00022-9

Rutqvist, J.: An overview of TOUGH-based geomechanics models. Comput. Geosci. 108, 56–63 (2017). https://doi.org/10.1016/j.cageo.2016.09.007

Schulze, O., Popp, T., Hartmut, K.: Development of damage and permeability in deforming rock salt. Eng. Geol. 61, 163–180 (2001). https://doi.org/10.1016/S0013-7952(01)00051-5

Settari, A., Mourits, F.: A coupled reservoir and geomechanical simulation system. SPE J. 3(3), 219–226 (1998). https://doi.org/10.2118/50939-PA

Stauffer, P.H., Harp, D.A., Jordan, A.B., Lu, Z., Kelkar, S., Kang, Q., Ten Cate, J., Boukhalfa, H., Labyed, Y., Reimus, P.W., Caporuscio, F.A., Miller, T.A., Robinson, B.A.: Coupled model for heat and water transport in a high level waste repository in salt. LANL. Rep. LANL M2FT-13L A08180113 (2013)

Stephansson, O., Hudson, J., Jing, L.: Coupled Thermo-Hydro-Mechanical-Chemical Processes In Geo-Systems: Fundamentals, Modelling, Experiments, and Applications. Geo-Engineering Book Series, vol. 2. Elsevier, London (2004)

Tsang, C.-F.: Coupled hydromechanical-thermomechanical processes in rock fractures. Rev. Geophys. 29(4), 537–551 (1991). https://doi.org/10.1029/91RG01832

Tsang, C.-F., Stephansson, O., Jing, L., Kautsky, F.: DECOVALEX Project: from 1992 to 2007. Environ. Geol. 57, 1221–1237 (2009). https://doi.org/10.1007/s00254-008-1625-1

Vaughan, P.J.: Analysis of permeability reduction during flow of heated, aqueous fluid through westerly granite. In: Tsang, C.F. (ed.) Coupled Processes Associated with Nuclear Waste Repositories, pp. 529–539. Academic Press, New York (1987)

Vargaftik, N.B.: Tables on the Thermophysical Properties of Liquids and Gases, 2nd edn. Hemisphere Publishing, New York (1975). https://doi.org/10.1002/aic.690210636

Verma, A., Pruess, K.: Thermohydrologic conditions and silica redistribution near high-level nuclear wastes emplaced in saturated geological formations. J. Geophys. Res. 93(B2), 1159–1173 (1988). https://doi.org/10.1029/JB093iB02p01159

Walker, W.R., Sabey, J.D., Hampton, D.R.: Studies of heat transfer and water migration in soils. Department Agric. Chem. Eng., Colorado State University. Final Rep. (1981)

Wang, W., Kosakowski, G., Kolditz, O.: A parallel finite element scheme for thermo-hydro-mechanical (THM) coupled problems in porous media. Comput. Geosci. 35, 1631–1641 (2008). https://doi.org/10.1016/j.cageo.2008.07.007

Wieczorek, K., Czaikowski, O., Zhang, C.L., Stührenberg, D.: Recent experimental and modeling results on crushed salt consolidation. In: Proceedings of 3rd US/German Workshop Salt Repository Research, Design and Operation, Albuquerque (NM) (2012)

Wolters, R., Lux, K.-H., Düsterloh, U.: Evaluation of rock salt barriers with respect to tightness: influence of thermomechanical damage, fluid infiltration and sealing/healing. In: Proceedings of 7th International Conference on Mechanical Behavior Salt (SaltMech7), pp. 425–434 (2012)